PCCP

PAPER

View Article Online
View Journal | View Issue

Cite this: *Phys. Chem. Chem. Phys.*, 2019, **21**, 5941

Quantitative analysis of ^{14}N quadrupolar coupling using ^{1}H detected ^{14}N solid-state NMR†

James A. Jarvis,‡[a] Maria Concistre,[b] Ibraheem M. Haies,[bc] Richard W. Bounds,[b] Ilya Kuprov,[b] Marina Carravetta[b] and Philip T. F. Williamson*[a]

Received 9th October 2018,
Accepted 29th January 2019

DOI: 10.1039/c8cp06276e

rsc.li/pccp

Magic-angle spinning solid-state NMR is increasingly utilized to study the naturally abundant, spin-1 nucleus ^{14}N, providing insights into the structure and dynamics of biological and organic molecules. In particular, the characterisation of ^{14}N sites using indirect detection has proven useful for complex molecules, where the 'spy' nucleus provides enhanced sensitivity and resolution. Here we exploit the sensitivity of proton detection, to indirectly characterise ^{14}N sites using a moderate rf field to generate coherence between the ^{1}H and ^{14}N at moderate and fast-magic-angle spinning frequencies. Efficient numerical simulations have been developed that have allowed us to quantitatively analyse the resulting ^{14}N lineshapes to determine both the size and asymmetry of the quadrupolar interaction. Exploiting only naturally occurring abundant isotopes will aid the analysis of materials with the need to resort to isotope labelling, whilst providing additional insights into the structure and dynamics that the characterisation of the quadrupolar interaction affords.

Introduction

Nitrogen-14 has a natural abundance of >99.6% and a moderate gyromagnetic ratio ($\gamma_{^{14}N}/\gamma_{^{1}H} \sim 0.07$), making it a potentially attractive nucleus for high-resolution solid-state NMR studies of nitrogen containing compounds. However, ^{14}N is a spin-1 nucleus with a nuclear quadrupole interaction (NQI) typically on the order of 1–5 MHz, making detection challenging. The NQI is however sensitive to variations in molecular symmetry, geometry and electrostatic environment, which in combination with its high natural abundance and prevalence in organic and biological materials, makes the development of methods to characterize ^{14}N sites desirable. To this end, a number of methods have been presented in the literature, particularly within the last ten years, that facilitate the determination of NQI parameters of nitrogen sites in a range of organic, biological and pharmaceutical materials.

Despite the size of the NQI and the width of resulting signal, ultra-wideline excitation methods developed by Schurko and co-workers have provided accurate NQI parameters at ^{14}N sites in a number of organic and pharmaceutical compounds.[1–3] The resolution of this method is inherently limited by the width of static ^{14}N signals, which overlap and hinder interpretation, limiting this technique to compounds with few (currently fewer than 3) unique ^{14}N sites.

Methods for detection of overtone ($\Delta m = \pm 2$) transitions on static samples,[4–6] and more recently under MAS[7–12] and DOR[13] have provided alternative methods for characterizing ^{14}N sites. Unlike $\Delta m = \pm 1$ ^{14}N signals, overtone signals are not affected by the large (MHz) quadrupole broadening. However, there are sensitivity concerns when exciting this "forbidden" transition, which are further exacerbated by the slow nutation and correspondingly low excitation bandwidth of overtone signals, making simultaneous detection of multiple ^{14}N overtone signals difficult.[8]

A third strategy for detection of ^{14}N is the indirect detection method, pioneered independently by Gan and Bodenhausen's laboratories,[14–25] where ^{14}N sites are detected *via* their interaction with coupled spin-1/2 'spy' nuclei; typically ^{1}H or ^{13}C, using pulse sequences qualitatively similar to HMQC experiments. Transfer of polarisation between the ^{14}N and the 'spy' nucleus occurs due to high-order cross-terms between the quadrupolar and ^{14}N'spy' dipolar Hamiltonians, known as the 'residual dipolar splitting' (RDS), as well as a contribution from the *J*-coupling, in experiments known as *J*-HMQCs. Alternatively, polarisation transfer can be driven by the recoupling of the ^{1}H/^{14}N dipolar coupling using rotary resonance (R^3), REDOR or symmetry based recoupling sequences, in sequences that have been generally termed *D*-HMQC experiments.[19,26,27] Similarly, double cross-polarization schemes have also been proposed for

[a] *Centre for Biological Sciences, University of Southampton, SO17 1BJ, Southampton, UK. E-mail: P.T.Williamson@soton.ac.uk*
[b] *School of Chemistry, University of Southampton, SO17 1BJ, Southampton, UK*
[c] *Department of Chemistry, College of Science, University of Mosul, Mosul, Iraq*

† Electronic supplementary information (ESI) available. See DOI: 10.1039/c8cp06276e

‡ Current address: Department of Life Sciences, Imperial College, SW7 2AZ, London, UK.

indirect detection which function well at higher spinning speeds.[28] These indirect techniques benefit from the sensitivity and resolution that are afforded by the 'spy' nuclei and do not require excitation or detection of the entire first-order broadened ^{14}N spectrum. Accordingly, they have found application to the study of structure and dynamics of a number of systems.[18,29,30] One of the major obstacles to the more widespread application of these techniques is their relatively poor spy nucleus/^{14}N transfer efficiencies, which usually result in a ~90% drop in sensitivity compared to the ^{1}H spin-echo, and the strong dependency on high ^{14}N RF amplitudes,[31] this is particularly acute at moderate spinning speeds (<60 kHz). This, in turn, renders the accurate *de novo* determination of ^{14}N NQI parameters from these experiments difficult, since precise determination of the quadrupolar coupling constant (C_Q) and asymmetry parameter (η) requires fitting of the ^{14}N lineshape, which cannot be achieved without high quality spectra with a high S/N ratio.

In this study we present a method for indirect detection of ^{14}N signals *via* ^{1}H's with enhanced efficiency at moderate to fast MAS frequencies (35–70 kHz), with transfer efficiencies of up to 27.5%, enabling acquisition of ^{1}H/^{14}N correlation spectra with improved signal/noise ratios and well-defined lineshapes in the ^{14}N dimension. This method, which is derived from our earlier work on the detection of ^{14}N *via* ^{13}C,[32] differs from previously published methods of indirect ^{14}N detection based on the HMQC pulse sequence, in that polarisation transfer occurs not under free evolution or established methods of heteronuclear dipolar recoupling, but rather under relatively long (100s μs) periods of moderate (30–70 kHz) RF irradiation on the ^{14}N channel (see Fig. 1). As described in our earlier studies, during these periods of irradiation both single and double quantum coherences are generated with efficiencies in excess of 20% of the initial equilibrium magnetization.[32] As per previous indirect detection sequences the indirect ^{14}N signals in 2D spectra are not affected by the typically large (MHz) first order quadrupolar interaction providing that the t_1 increments are rotor synchronised and the magic-angle accurately set. This results in ^{14}N signals at a frequency which is the sum of the chemical shift and second order isotropic quadrupolar shift (δ_Q^{iso}), given for the general case in ppm by:[29]

$$\delta_Q^{iso} = \left\{ -\left(\frac{3}{40}\right)\left(\frac{\chi_q}{\upsilon_0}\right)^2 \frac{[I(I+1) - 9m(m-1) - 3]}{[I^2(2I-1)^2]} \right\} \times 10^6 \quad (1)$$

where I and m are the spin quantum numbers and υ_0 is the Larmor frequency in Hz. Eqn (1) simplifies to:

$$\delta_Q^{iso} = \left(\frac{3}{40}\right)\left(\frac{\chi_q}{\upsilon_0}\right)^2 \times 10^6 \quad (2)$$

In the case of ^{14}N, when $I = 1$ and $m = +1$ or 0. The quadrupolar product, χ_q, is given by:

$$\chi_q = C_Q\sqrt{1 + (\eta^2/3)} \quad (3)$$

If the isotropic chemical shift, δ_{CS}^{iso}, is known, for example from studies of ^{15}N spectra, then the ^{14}N δ_Q^{iso} contribution to the ^{14}N shift of a given peak can be determined by subtraction of the ^{15}N δ_{CS}^{iso} from the observed ^{14}N shift, allowing the determination of χ_q. Previous studies have shown the experimentally measured χ_q to be consistent with previously determined or calculated values of C_Q and η for glycine and peptides of AGG and β-DA,[14,16,30] and has been used to investigate H-bonding in pharmaceuticals.[29] However, in order to quantitatively determine C_Q and η precisely from such data, η must be determined by fitting the ^{14}N lineshape to simulations.

The simulation of indirectly detected ^{14}N lineshapes is difficult since the lineshape depends on numerous parameters, including quadrupolar broadening, and the orientation of the quadrupolar tensor with respect to the dipolar and CSA tensors. Therefore, determination of ^{14}N NQI parameters has not been previously attempted due to (a) poor efficiency of indirect detection methods leading to noisy and ill-defined ^{14}N lineshapes unsuitable for fitting, and (b) computationally expensive nature of simulating these experiments. In this work, we address both of these issues and present a highly efficient ^{1}H/^{14}N correlation experiment, and fast and accurate simulations which in combination allow the *de novo* determination of ^{14}N NQI parameters from organic solids with a variety of ^{14}N sites with various NQI parameters. These fast and accurate numerical simulations of each ^{14}N site allows the fitting of simulations to experimental lineshapes and the simultaneous determination of ^{14}N NQI parameters at multiple sites from a 2D data set.

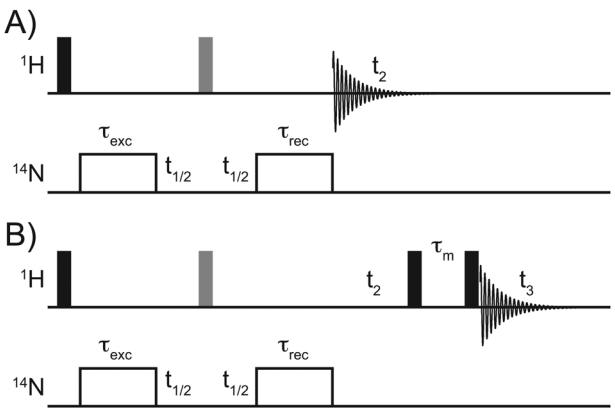

Fig. 1 Pulse sequences employed for the acquisition of the 2D-^{14}N/^{1}H (A) and 3D-^{14}N/^{1}H/^{1}H correlation (B) spectra reported in this study. The length of the excitation (τ_{exc}) and reconversion pulses (τ_{rec}) and the t_1 increments are chosen to ensure that the sequence is rotor synchronised, π/2 and π pulses are highlighted in black and grey respectively. For the 3D experiment, proton mixing during τ_m was conducted using a RFDR pulse train, pulses have been omitted for clarity.

Materials and methods

Materials

Samples of histidine hydrochloride monohydrate (His·HCl·H_2O), L-histidine (L-His), *N*-acetyl-valine (NAV) and valine were purchased from Sigma-Aldrich (UK) and used without further purification.

Solid-state NMR experiments

Solid-state NMR experiments on His·HCl·H_2O and L-His were performed on an Agilent DDR2 spectrometer operating at 14.1 T (Larmor frequencies of 600 MHz and 43.4 MHz for ^{1}H and ^{14}N) equipped with a 1.6 mm triple resonance MAS probe tuned in double resonance mode. MAS frequencies were 40 kHz for the L-His sample and 35.5 kHz for the His·HCl·H_2O sample.

The pulse sequence for indirect detection of ^{14}N *via* ^{1}H used in this work is shown in Fig. 1. Pulse lengths for ^{1}H pulses were $\pi/2$ = 1.55 μs, π = 3.10 μs on both samples, ^{14}N pulses for excitation and reconversion were applied at 62.5 kHz for 575 μs, and 30 kHz for 390 μs for L-His and His·HCl·H_2O, respectively. The L-His spectrum was recorded with 112 scans per t_1 increment, with 160 complex increments and a recycle delay of 2 s and the His·HCl·H_2O spectrum was recorded with 64 scans and 254 t_1 increments with a recycle delay of 2 s. Both were recorded using States-TPPI.[33] Both datasets were zero-filled to 2048 × 2048 points and 2D Fourier transformed without a window function.

Experiments on NAV were performed on a Bruker Avance II spectrometer at 20 T (Larmor frequencies of 850 MHz and 61.4 MHz for ^{1}H and ^{14}N) using a JEOL 1 mm double resonance MAS probe. The sample was spun with a MAS frequency of 78 kHz. Spectra were acquired using the pulse sequence in Fig. 1. ^{1}H pulses were $\pi/2$ = 1.1 μs, π = 2.2 μs and ^{14}N excitation and reconversion pulses were applied at 72 kHz for 370 μs. 128 complex t_1 increments were recorded with 136 scans per increment, in a phase sensitive manner, using States-TPPI.[33] The recycle delay was 3 s. Data was zero-filled to 2048 points in each dimension before 2D Fourier transform. 3D ^{14}N resolved ^{1}H/^{1}H correlation spectra were acquired the pulse scheme shown in Fig. 1B. Following ^{14}N evolution, protons were allowed to evolve under the proton chemical shift prior a period of RFDR proton/proton mixing[34] prior to detection. Data was acquired with States-TPPI[33] in both indirect dimensions with 16 and 32 increments in the indirect ^{14}N and ^{1}H dimensions respectively. Data was processed in nmrPipe[35] and visualised in Analysis 2.4.0, modified to include ^{14}N parameters.[36] In all spectra, the ^{14}N dimension is referenced to the ^{14}N resonance of NH_4Cl at 39.3 ppm, ensuring that the ^{14}N shifts can be compared directly with values on the scale typically used for referencing ^{15}N in biological solids.[37]

Numerical simulations

All NMR simulations were performed with the *Spinach* library versions 1.6 and 2.2.[38] Each nitrogen site simulated was approximated as a pair of nuclei comprising the ^{14}N nucleus and the closest bound proton. Simulations included dipolar coupling, CSA and NQI parameters for both spins that were initially obtained from CASTEP calculations[39] or literature values. These initial calculated and literature values are shown in Table 1. Relative orientations of ^{14}N NQI and ^{14}N and ^{1}H CSA tensors were also obtained from the literature, and are also given in Table 1, defined with respect to the PAS of the ^{1}H–^{14}N dipolar tensor. Relaxation was neglected in the simulations, and an apodization function applied to simulated FIDs before Fourier transform that reflected the effective T_2 of the experimental ^{14}N signal. An input script for the experiment described in this paper is available in the latest release of the *Spinach* library. For simulations on sites in L-His and His·HCl·H_2O, powder averaging was performed over 770 pairs of α and β angle orientations calculated using the Lebedev method. A Floquet rank of 45 was sufficient for convergence for all sites in L-His and His·HCl·H_2O except the N_δ site of His·HCl·H_2O, where a rank of 55 was required due to the increased C_Q magnitude. Simulations of NAV used 1454 α and β angle orientations and a Floquet rank of 55. To fit the experimentally determined lineshapes the simulated ^{14}N signals, C_Q and η were systematically varied in steps of 50 kHz and 0.1 respectively and the RMSD between experiment and simulation calculated.

CASTEP calculations

To calculate the NQI we used the CASTEP density function theory (DFT) package[39–42] which uses the gauge including projector augmented wave (GIPAW) algorithm. We used the Perdew–Burke–Ernzerhof (PBE) generalised gradient approximation (GGA) with ultrasoft pseudopotentials and 0.1k points Å^3. We tested the value of the NQI by converging against the plane-wave energy cut-off tolerance.

Results and discussion

Histidine hydrochloride monohydrate and L-histidine

In order to assess the effects of alternate hydrogen bonding patterns and changes in local geometry on ^{14}N NQI parameters

Table 1 Parameters describing the spin interactions and their relative geometries found in the compounds used in this study

Sample	Site	δ (ppm)	C_Q (MHz)	η	Orientation (α, β, γ)		
					^{14}N C_Q	^{14}N CSA	^{1}H CSA
His·HCl·H_2O	NH_3^+	47.3[a,d]	1.32[c]	0.06	0, 0, 0	—	109, 72, 172
	N_δ	189.8[a,d]	1.53[c]	0.23	0, 90, 0	−71.18, 1.5, −7.2	102.1, 66, −84
	N_ε	177.2[a,d]	1.33[c]	0.94		−75, 181.5, −7.2	90, 196, −86
L-His	NH_3^+	41.6[a]	1.22[b]	0.15	0, 0, 0	—	109, 72, 172
	N_ε	168.9[a]	1.44	0.92	0, 90, 0	75, 181.5, −7.2	90, 196, −86
NAV	N1	127.7	3.21[f]	0.32	13.2, 90, 103[g]	51, 20, 0[e]	103.2, 0, 193[h]

[a] Measured on ^{15}N using CPMAS. [b] Ref. 7. [c] Calculated values using CSD reference code: HISTCM12. [d] Ref. 43 and 44. As referenced to NH_4Cl at 39.3 ppm. [e] Ref. 45–47. As referenced to NH_4Cl at 39.3 ppm. [f] Ref. 48. [g] Ref. 49. [h] Ref. 50.

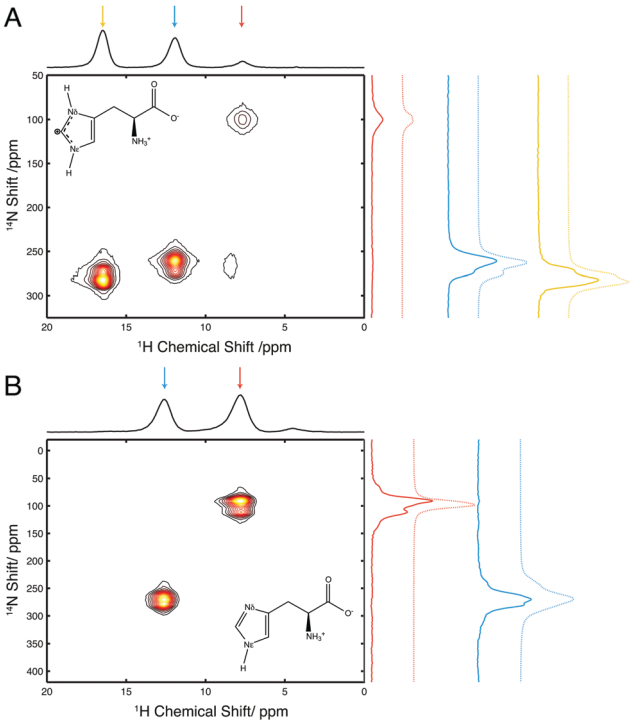

Fig. 2 ^{1}H/^{14}N correlation spectra of two forms of histidine at 14.1 T. Spectrum of His·HCl·H_2O recorded at 35.5 kHz (A) MAS frequency L-His spectrum (B). Recorded at 40 kHz MAS frequency. Experimental (solid) and simulated (dashed) projections through the ^{14}N dimension are plotted for each spectrum at the NH_3^+ site (red), the N_ε site (blue) and the N_δ site (yellow). The projections are normalised to the maximum peak intensity in each respective spectrum.

at a number of different nitrogen sites, and how these changes affect ^{14}N lineshapes and peak positions, we initially investigated samples of L-His and His·HCl·H_2O. These two salts of histidine exhibit different protonation states (see Fig. 2) and H-bonding networks, resulting in a variation in local electronic structure with the associated variation in ^{14}N NQI parameters (Table 1).

Fig. 2A shows the ^{1}H/^{14}N correlation spectrum of His·HCl·H_2O, recorded at 14.1 T, under 35.5 kHz MAS. Three peaks are observed, corresponding to the three protonated nitrogen sites in this molecule. The NH_3^+, N_δ and N_ε and sites appear at ^{14}N shifts of 100 ppm, 263 ppm and 280 ppm, respectively. The transfer efficiency of this experiment was 27.5% at N_ε, 24.4% at N_δ and 7.5% at NH_3^+ sites, expressed relative to a ^{1}H spin echo on the same sample using delays equal to the length of applied ^{14}N pulses. These efficiencies are comparable with or in excess of those reported in the literature for the same or similar compounds acquired with both *J*- and *D*-HMQC sequences. Using the *J*-HMQC sequence under ultrafast MAS (90 kHz), which is optimal for the ^{1}H detected *J*-HMQC sequence since ^{1}H coherence lifetimes that these experiments are particularly sensitive to increase significantly with MAS, ^{14}N transfer efficiencies of 7.55% and 9.75% with respect to ^{1}H spin echo were recently reported for the N_ε and N_δ sites in His·HCl·H_2O.[51] Using a *D*-HMQC sequence, with R^3 recoupling, transfer efficiencies of 5–6% have been reported for the NH_3^+ site in glycine at 20 kHz MAS.[16] The experiment performed here was optimised (in terms of ^{14}N offset and pulse length) such that efficiency was maximally distributed over the two heterocyclic ^{14}N sites, and as such, ^{14}N pulse widths and amplitudes are possible that increase the efficiency at any of the three sites, at the expense of signal intensity at the other sites. This results in a spectrum with a quality and signal/noise ratio such that subtle spectral features such as the shoulders on the peaks of N_ε and N_δ are observed which can aid in the characterisation of the quadrupolar interaction.

Fig. 2B shows a ^{1}H/^{14}N correlation spectrum of L-His, recorded at 14.1 T under 40 kHz MAS. In this spectrum only two peaks are observed which are the NH_3^+ and N_ε sites at 100 ppm and 278 ppm ^{14}N shifts, respectively; the unprotonated N_δ site is not detected. Similar transfer efficiencies were achieved as those for His·HCl·H_2O, with 20.0% and 16.6% of ^{1}H spin echo signal recorded at N_ε and NH_3^+ sites, respectively. This experiment was optimised for an even distribution of intensity between the two ^{14}N sites and could be optimised to achieve a higher signal intensity at one site, potentially at the expense of that at the other.

Comparing the peaks from the N_ε and NH_3^+ sites in L-His to the peaks from the same sites in His·HCl·H_2O, there are differences in both ^{14}N frequency and peak shape. The ^{14}N frequency may be used to determine ^{14}N δ_Q^{iso} at each site. Contributions from the ^{14}N chemical shift and ^{14}N δ_Q^{iso} to the observed ^{14}N shift at each peak in the spectra of L-His and His·HCl·H_2O are separated by subtracting the contribution from the isotropic chemical shifts, which are shown in Table 1. These were determined from a separate natural abundance ^{15}N CPMAS experiment performed on each sample. For both materials, the measured values of ^{14}N δ_Q^{iso} are tabulated in Table 2.

The δ_Q^{iso} can be used to estimate the magnitude of the C_Q and η at each site, using eqn (1)–(3). A contour plot of values of δ_Q^{iso} at 14.1 T, calculated from eqn (1), as a function of the magnitude of the C_Q and η are shown in Fig. S1 (ESI†). As expected from eqn (2), C_Q and η are correlated, however at this field the δ_Q^{iso} shows only a limited dependence on the asymmetry parameter η and thus C_Q can be readily constrained to a range of ~200 kHz irrespective of the asymmetry parameter. In L-His the NH_3^+ and N_ε sites are determined to have C_Q tensor magnitudes of 1.00–1.15 MHz and 1.37–1.58 MHz respectively, and the NH_3^+, N_ε and N_δ sites in His·HCl·H_2O have magnitudes of 1.00–1.15 MHz, 1.28–1.48 MHz and 1.32–1.52 MHz, for all

Table 2 Calculated and experimental ^{14}N δ_Q^{iso} values for the samples used in this study

Sample	Site	δ_Q^{iso} expt.[a] (ppm)	δ_Q^{iso} calc.[b] (ppm)
His·HCl·H_2O	NH_3^+	55.4	69.5
	N_δ	90.2	94.9
	N_ε	85.8	91.1
L-His	NH_3^+	58.4	59.7
	N_ε	105.4	105.9
NAV	N1	207.1	211.5

[a] The centre of gravity of the ^{14}N peak in the indirect dimension – ^{15}N δ_{CS}^{iso} from Table 1. A ±5 ppm error is associated with measuring the ^{14}N frequency from the spectra. [b] Calculated from C_Q and η from Table 1 using eqn (2), with Larmor frequencies calculated from B_0 = 14.1 T for histidine sites, and B_0 = 20.0 T for NAV.

possible values of η. The C_Q of the NH_3^+ site in both compounds can be constrained to a smaller range of C_Q magnitudes, since χ_q and, therefore, ^{14}N δ_Q^{iso} is less dependent on η when the C_Q is smaller. The agreement of the ^{14}N δ_Q^{iso} determined from indirect detection methods in this paper, as compared to those calculated from literature values for ^{14}N chemical shift and NQI tensors in the histidine compounds studied here is demonstrated in Table 2. In general, the ^{14}N δ_Q^{iso} observed in this work is smaller than that expected from literature values obtained by other techniques, or CASTEP calculated values. This discrepancy is most severe at the amine sites of both histidine molecules, with the His·HCl·H_2O experimental NH_3^+ ^{14}N δ_Q^{iso} being 14.1 ppm lower than the calculated value, and that site in L-His was found to be 9 ppm lower than the literature/calculated value. At the remaining heterocyclic sites, the N_ε site in His·HCl·H_2O was found to deviate most from the ^{14}N δ_Q^{iso} value calculated from literature NQI parameter values, at 5.3 ppm. These deviations, being most severe for the highly mobile primary amine sites in histidine compounds, may be due to comparisons being made with NQI parameters determined by different techniques at cryogenic temperatures rather than room temperature, freezing out motions that could scale the ^{14}N NQI in our experiments, or comparisons with CASTEP calculations that do not take into account molecular motions.

Quantitative analysis of histidine spectra

Having recorded indirect ^{14}N detected spectra with very high efficiencies, the quality of data was high enough to observe subtle spectral features in the ^{14}N lineshapes, for example, the shoulders on the sides of N_ε and N_δ peaks in the His·HCl·H_2O spectrum. As it is not possible to accurately determine C_Q and η from the quadrupolar product alone, a more accurate analysis was undertaken fitting the ^{14}N lineshapes in the indirect dimension. Numerical simulations were fitted to the experimentally determined lineshapes at each ^{14}N site in the two histidine compounds, by systematically searching a C_Q and η parameter space spanning $C_Q = \pm 0.25$ MHz and $\eta = \pm 0.25$ of the published or calculated values. Plots of the root mean squared deviation (RMSD) between simulated and experimental spectra for each of the ^{14}N sites in the histidine samples studied is shown in Fig. 3. The fits of these lineshapes were conducted with the quadrupolar and chemical shielding tensors oriented with respect to the $^1H/^{14}N$ dipolar coupling according the values given in Table 1. Simulations indicate that these parameters do indeed contribute to the overall $^1H/^{14}N$ lineshape, however for compounds with a small C_Q these effects are negligible with the linewidths that are experimentally obtainable.

There is a strip of relatively good agreement (RMSD $< \sim 0.3$) through the RMSD plot for each ^{14}N site where the simulated ^{14}N δ_Q^{iso} is consistent with that observed experimentally. A single black contour line through each plot marks the experimentally observed ^{14}N δ_Q^{iso}, which are also plotted on the contour plot in Fig. S1 (ESI†), and tabulated in Table 2. This line generally coincides with the area of lowest RMSD in each plot. This shows that the largest contribution to the quality of the simulations fit is determined from the ^{14}N δ_Q^{iso}, which is to be expected since it

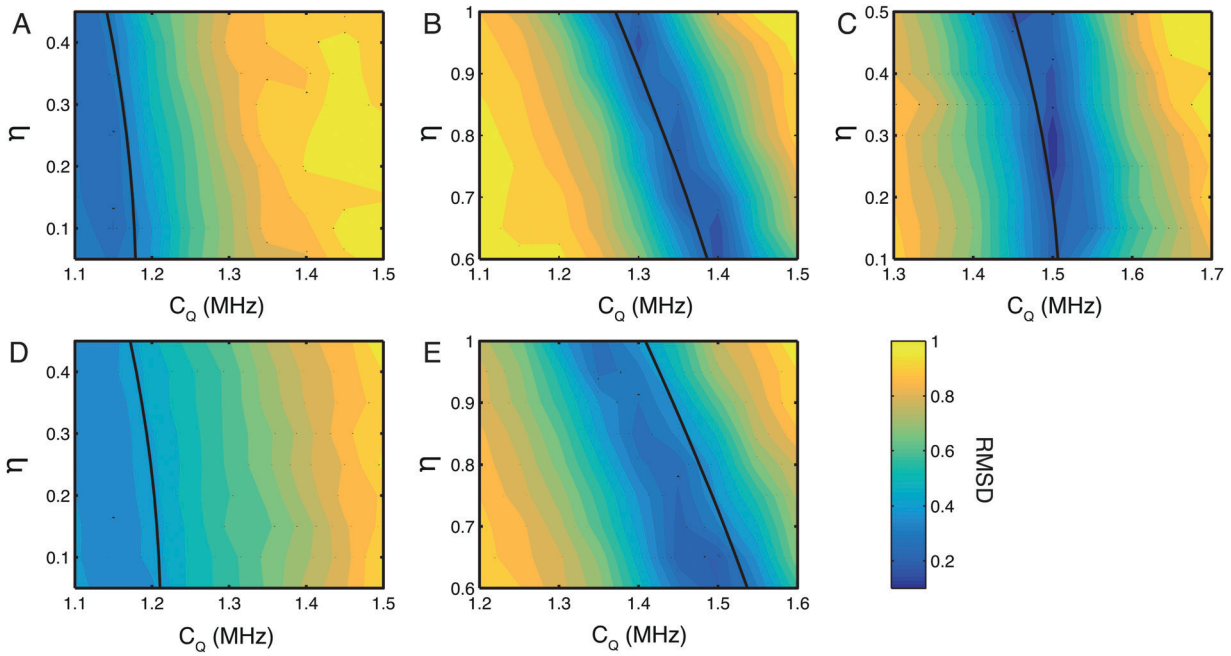

Fig. 3 RMSD plots of simulated and experimental ^{14}N lineshapes. Plots for the NH_3^+ (A) N_ε (B) and N_δ (C) sites in His·HCl·H_2O and the NH_3^+ (D) and N_ε (E) sites in L-His. The magnitude of the C_Q was arrayed in steps of 0.05 MHz from −0.25 to +0.25 MHz from the initial value, and η was arrayed in steps of 0.05 from −0.25 to +0.25 about a region spanning the predicted η for each nitrogen site based on the figures in Table 1. In all cases, contour lines are spaced by 5% of the maximum RMSD value. Errors estimated at the 10% RMSD level are $C_Q = 1.1 \pm 0.3$ MHz, $\eta = 0.3 \pm 0.3$ for (A), $C_Q = 1.4 \pm 0.08$ MHz, $\eta = 0.64 \pm 0.04$ for (B), $C_Q = 1.5 \pm 0.1$ MHz, $\eta = 0.26 \pm 0.06$ for (C), C_Q 1.1 ± 0.3 and η poorly defined (see text for discussion) for (D), $C_Q = 1.4 \pm 0.15$ MHz, $\eta = 0.90 \pm 0.06$ for (E). The single black contour line in each plot indicates the δ_Q^{iso} for each site calculated from the measured ^{14}N shift δ_Q^{iso}.

determines the position of the peak. In the RMSD plot for the N_δ of His·HCl·H_2O, Fig. 3C, a single RMSD minimum where the RMSD is <0.15 (darkest blue contours) is observed. This covers a range of C_Q = 1.49–1.51 MHz, and η = 0.22–0.34, which is in close agreement with the CASTEP calculated values at this site, C_Q = 1.53 MHz, and η = 0.23, as well as literature values of C_Q = 1.47 MHz, and η = 0.27.[52] Additionally, visual comparison of the simulated lineshape with the experimental lineshape (Fig. 2A, yellow traces) shows a good agreement. This plot demonstrates that using a simulation fitting approach, one can define η to a range of $\sim\pm0.1$, which allows the C_Q to be determined with a precision of tens of kHz, which is at least an order of magnitude more precise than one can achieve considering only the ^{14}N δ_Q^{iso}.

In the RMSD plots for the N_ε sites of both His·HCl·H_2O (Fig. 3B) and L-His (Fig. 3E), the fit of the lineshape with respect to η is somewhat less robust. In the case of the N_ε site in His·HCl·H_2O, two RMSD minima <0.2 are observed, at C_Q = 1.29–1.3 MHz, η = 0.93–0.97, and C_Q = 1.39–1.41 MHz, η = 0.60–0.68. The former of these minima, however, is consistent with the calculated values for this site, of C_Q = 1.33 MHz, η = 0.94, as well as reported literature values of C_Q = 1.29 MHz, η = 0.95.[52] For the N_ε site in L-His, the same general pattern is observed, with two RMSD minima in similar positions with respect to η as those observed at the same site in His·HCl·H_2O (C_Q = 1.35 MHz, η = 0.95–1.00, and C_Q = 1.5 MHz, η = 0.60–0.65). However, the fit is not as good as that of the N_ε site in the hydrochloride salt; in L-His the RMSD minima are broader, and the RMSD is not as low (minimum RMSD = 0.24). This is probably due to there being less well-defined features in the experimental lineshape at this site (as shown in Fig. 2B) compared to the N_ε in His·HCl·H_2O (Fig. 2A). However, the N_ε sites are expected to have similar chemical environments and hydrogen bond geometries, and therefore similar ^{14}N spectral parameters in terms of their ^{14}N EFG and CSA tensors which give rise to the features observed in the ^{14}N lineshapes, and one of the RMSD minima (at C_Q = 1.35 MHz, η = 0.95–1.00) is consistent with expected values.

The NH_3^+ sites in both His·HCl·H_2O and L-His show a poor fit of the simulated lineshape with respect to η, with the minimum RMSD encompassing almost the whole range of η values simulated, and not falling below RMSD = 0.3. This means it is not possible to use these plots to constrain the C_Q at either site more precisely than was achieved by considering simply the ^{14}N δ_Q^{iso}.

In the case of the His·HCl·H_2O the rather poorly defined minima reflects the featureless nature of the peak without any discontinuities, shoulders or splittings, making a distinctive fit difficult. This may be due to the fast ^1H T_2* decoherence at this site leading to a broadening of the signal and the loss of any distinctive features, indeed simulated spectra exhibited well defined splittings and shoulders before the application of the apodization to match the experimentally observed decay. We attribute this rapid relaxation to the molecular motions present at the site,[53–55] which, in the case of NH_3^+ groups have previously been shown to influence the SQ ^{14}N lineshape.[18]

At the NH_3^+ site in L-His, a well-defined splitting was observed in the ^{14}N lineshape. However, the fit of the simulated spectra to this lineshape was the least satisfactory of all those investigated here, with a minimum RMSD = 0.35. As the experimental and simulated slices (Fig. 2B, red traces) show, the experimental spectrum observed was significantly broader, with more features, than the best fit simulated spectrum. The reason for this may be that at the NH_3^+, the ^{14}N is coupled to three separate protons, which cannot be resolved in the ^1H spectrum, and so their contributions to the ^{14}N lineshape are superimposed in the ^{14}N dimension. The simulated lineshape only takes into account an approximation of the spin system with ^{14}N coupled to a single amine proton. This would mean that the simulation only accounted for part of the experimental lineshape, and that the remaining features were due to coupling to the other protons at the NH_3^+. Similar effects could also arise through the presence of conformational disorder in the sample or the presence of multiple polymorphs.

The differences observed between the fitted NH_3^+ lineshape and those experimentally obtained may also reflect the limitations of our current simulations which ignore the effects of relaxation and motional processes. Although such effects could be incorporated into the calculations, these simulations are already computationally demanding and, practically, close to the limit of what we can achieve in a reasonable timeframe (several weeks of supercomputer time) when fitting a grid of parameters to experimental data. In contrast; fits of the heterocyclic ^{14}N sites exhibit a better fit with the experimental data, with the C_Q and η in good agreement with published or calculated values. This is particularly clear for the N_δ site where the larger C_Q is larger.

N-Acetyl-valine spectrum

Further proton detected experiments were performed on NAV (see Fig. 4), which exhibits a larger NQI than the sites studied in the histidine samples, with a C_Q of 3.21 MHz and a η = 0.32,[48] and as such mirrors the properties of ^{14}N sites within the peptide bonds of proteins and peptides.[56] Fig. 4A shows a 2D $^1H/^{14}N$ correlation spectrum recorded on a sample of NAV at 20.0 T (850 MHz ^1H Larmor frequency) and a MAS frequency of 78 kHz. Experiments were performed at a higher field with ultra-fast MAS in order to optimise conditions for proton detection on this challenging, high-C_Q sample. The increased field and MAS frequency, significantly enhances the sensitivity of the experiment, lengthening coherence lifetimes and reducing the ^1H homogeneous linewidth. The ^{14}N shift of the amide ^{14}N in NAV at this field is 335 ppm. From this shift, a ^{14}N δ_Q^{iso} = 207.3 ppm is calculated, by subtracting the δ_{cs}^{iso} of 127.7 ppm (measured by ^{15}N CPMAS). This agrees well with the expected ^{14}N δ_Q^{iso} value of 211.5 ppm calculated for this field from literature values.[48] The efficiency of the two-way ^{14}N transfer is 9% with respect to the ^1H spin echo signal under the same conditions. This is lower than the efficiencies of the proton detected experiment generally observed on the lower magnitude C_Q sites in the histidine compounds. This is a trend observed in all indirect ^{14}N detection experiments and can be attributed to

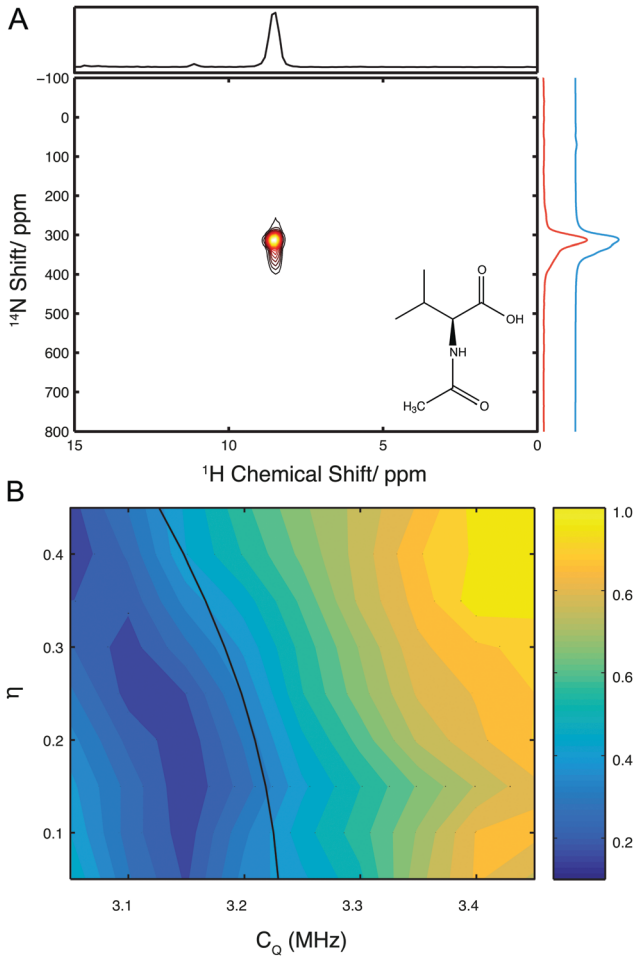

Fig. 4 ^{1}H/^{14}N correlation spectrum of NAV at 20 T. Spectrum of NAV recorded at 78 kHz MAS. Experimental (red) and simulated (blue) projections through the ^{14}N dimension are shown. (A) Plot of RMSD between experimental and simulated spectra of NAV at 20 T (B).

the increased magnitude of the ^{14}N C_Q in NAV, which is likely to mean that the pulses applied on the ^{14}N channel excite the far broader ^{14}N spectrum to a lesser extent.

Quantitative analysis of *N*-acetyl-valine spectra

A quantitative analysis of the NAV was conducted in a similar manner to that utilized for the histidine compounds. A plot of the ^{14}N δ_Q^{iso}, calculated from eqn (2), as a function of C_Q and η at 20.0 T, with the experimentally measured NAV ^{14}N δ_Q^{iso} marked, is shown in Fig. S2 (ESI†). From this plot, one can read off the upper and lower limits placed on the C_Q at the ^{14}N site in NAV by the ^{14}N δ_Q^{iso} and determine the range of C_Q magnitudes consistent with the ^{14}N δ_Q^{iso} as 2.83–3.26 MHz, for all values of η. This range of 430 kHz is far larger than the range of ~200 kHz that could be obtained for the moderate C_Q (1.0–1.5 MHz) sites found in histidines at 14.1 T. This is since when the C_Q is large, the effects of η on the ^{14}N δ_Q^{iso} will be larger, as evident from eqn (2), since η and C_Q are correlated, and the contribution of η is scaled by the C_Q magnitude.

Fig. 4B shows a contour plot of the RSMD of simulated spectra with respect to the experimental ^{14}N lineshape in NAV as a function of the C_Q and η used in the simulations. A comparison of the best-fit ^{14}N simulated lineshape with the experimental lineshape is seen in the projections in Fig. 4. The quality of the fit is high, with a minimum RMSD = 1.5, however the RMSD minimum is relatively broad; covering a region of C_Q magnitude of 75 kHz (C_Q = 3.1 MHz–C_Q = 3.175 MHz), and range of η values of 0.32 (0–0.32). The range of values covered by this RMSD minimum slightly underestimates the literature values of C_Q = 3.21 MHz, η = 0.32.[48] However, the black contour line which indicates the ^{14}N δ_Q^{iso} calculated from the measured ^{14}N shift at the centre of gravity of the ^{14}N lineshape is also underestimated by the best RMSD fit, and in fact agrees very well with the literature values. The lack of accuracy with which the simulations fit the data suggest that there are features of the experimental ^{14}N lineshape that are not accounted for in the simulations. The reason for this is unclear. Simulations to ascertain if the relative orientations of the quadrupolar, dipolar and chemical shift anisotropy influenced the lineshape were conducted (see Fig. S3 and S4, ESI†). Simulations in the absence of the chemical shielding anisotropy (CSA) (Fig. S3, ESI†) show that the proton lineshape is strongly correlated to the β Euler angle describing the orientation of the quadrupolar tensor with respect to the ^{1}H/^{14}N dipolar coupling tensor, whilst the influence of the corresponding α Euler angle is limited to the lineshape. Similarly, introduction of the CSA into the simulations (Fig. S4, ESI†) resulted in minor changes to the lineshape. Although the effects of tensor orientation are pronounced when the linewidths are small, many of these factors are masked with the currently attainable experimental resolution, which together with the computationally demanding nature of the simulations and large parameter space precludes a more rigorous statistical fitting of the lineshape. Alternatively, it is plausible that the signal is broadened or shifted by higher-order terms (>2) in the quadrupolar Hamiltonian that are not accounted for in the simulations and not removed by MAS. For sites with lower (<1.5 MHz) quadrupolar couplings, it was verified that these terms did not affect the simulated lineshapes. However, this was not verified for the case where the quadrupolar coupling was large (~3 MHz) and high order terms are expected to be more significant, as running the simulations with the full Hamiltonian was found to be prohibitively time consuming. Finally, it may be that the ^{14}N spectrum of this site is broadened by high mobility of the amide nitrogen, although we acknowledge that this is not reflected in the size of the quadrupolar interaction.

Multidimensional ^{14}N correlation spectroscopy

The quadrupolar interaction provides a sensitive reporter of secondary structure within proteins, with variations of up to 200 kHz reported between alpha-helical and beta-sheet structures, corresponding to variation in δ_Q^{iso} of ~130 ppm in the proton detected spectra reported here. Despite the large variation in δ_Q^{iso} reported for proteins, for larger biomolecules its application will remain challenging due to the limited chemical shift dispersion in the amide protons. Although further enhancements in resolution and sensitivity can be realised through the

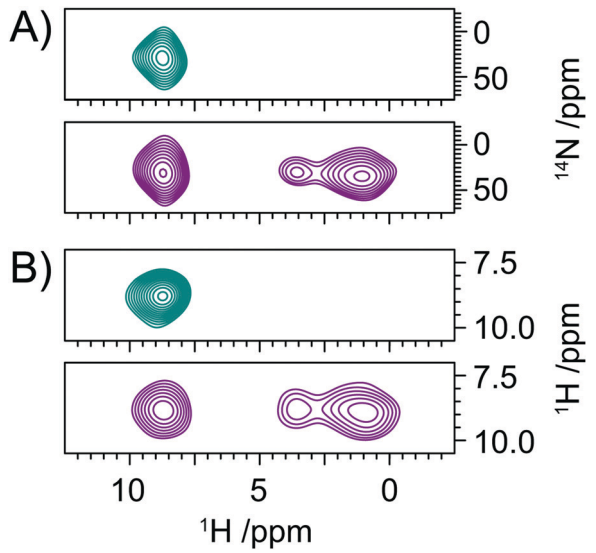

Fig. 5 Slices extracted from a 3D, ^{14}N resolved ^{1}H/^{1}H correlation spectrum of valine with no proton/proton mixing (teal), and 24 rotor cycles of RFDR mixing (purple). ^{1}H/^{14}N planes (A) and their respective ^{1}H/^{1}H planes (B).

application of faster MAS and higher ^{14}N rf fields,[26,32] for larger biomolecules it is clear that higher-dimensionality spectra will be required to aid resolution and assignment. In Fig. 1B we describe a 3D experiments which allows the acquisition of a ^{14}N resolved ^{1}H/^{1}H correlation experiment. Analogous in many ways to the ^{15}N filtered ^{1}H/^{1}H NOESY experiment frequently employed in the liquid state, the ^{1}H/^{1}H correlations are now resolved according to the δ_{Q}^{iso} of the adjacent ^{14}N site. The efficiency of the experiment ensures that such data sets can be acquired in as little as 2 days, with the overall duration limited by the phase cycling employed (Fig. 5).

Conclusions

We have demonstrated the application of a novel method of indirect detection of ^{14}N *via* ^{1}H under moderate and fast MAS frequencies, applied to two forms of histidine and NAV. Spectra with up to 27.5% efficiency can be recorded using this method, resulting in a large increase in S/N and spectral quality, over previous methods. The data presented have been fitted to simulated lineshapes to extract NQI parameters for nitrogen sites in different chemical environments with increased precision. The ^{1}H detected ^{14}N experiments described here are not as limited in the number of sites that can studied as previous methods such as piecewise detection, indeed the variation observed in C_Q served to enhance the resolution. Furthermore, exploitation of ^{1}H detection facilitates its application to unlabelled biomolecules, providing a viable route to study the structure and dynamics complex natural organic and biomolecular systems.

Conflicts of interest

There are no conflicts to declare.

Acknowledgements

This research was supported by The Wellcome Trust (PTFW and MC), EPSRC (EP/H003789/1, IK; EP/M023664/1, MC/PTFW/IK), The University of Southampton (JJ), and The Royal Society University Research Fellowship (MC). IK thanks EPSRC for an Impact Acceleration grant, and Jos Martin of MathWorks for technical support. IH thanks The Higher Committee for Education Development in Iraq for financial support. The UK 850 MHz solid-state NMR Facility instruments used in this research were funded by EPSRC and BBSRC, as well as the University of Warwick, including *via* part funding through Birmingham Science City Advanced Materials Projects 1 and 2 supported by Advantage West Midlands (AWM) and the European Regional Development Fund (ERDF). The authors acknowledge the use of the IRIDIS High Performance Computing Facility, and associated support services at the University of Southampton, in the completion of this work.

References

1 K. J. Harris, S. L. Veinberg, C. R. Mireault, A. Lupulescu, L. Frydman and R. W. Schurko, *Chemistry*, 2013, **19**, 16469–16475.
2 L. A. O'dell, R. W. Schurko, K. J. Harris, J. Autschbach and C. I. Ratcliffe, *J. Am. Chem. Soc.*, 2011, **133**, 527–546.
3 S. L. Veinberg, Z. W. Friedl, K. J. Harris, L. A. O'Dell and R. W. Schurko, *CrystEngComm*, 2015, **17**, 5225–5236.
4 R. Tycko and S. J. Opella, *J. Am. Chem. Soc.*, 1986, **108**, 3531–3532.
5 R. Tycko and S. J. Opella, *J. Chem. Phys.*, 1987, **86**, 1761.
6 R. Tycko, P. L. Stewart and S. J. Opella, *J. Am. Chem. Soc.*, 1986, **108**, 5419–5425.
7 L. A. O'Dell and A. Brinkmann, *J. Chem. Phys.*, 2013, **138**, 064201.
8 L. A. O'Dell, R. He and J. Pandohee, *CrystEngComm*, 2013, **15**, 8657.
9 L. A. O'dell and C. I. Ratcliffe, *Chem. Phys. Lett.*, 2011, **514**, 168–173.
10 A. J. Rossini, L. Emsley and L. A. O'Dell, *Phys. Chem. Chem. Phys.*, 2014, **16**, 12890–12899.
11 I. M. Haies, J. A. Jarvis, H. Bentley, I. Heinmaa, I. Kuprov, P. T. F. Williamson and M. Carravetta, *Phys. Chem. Chem. Phys.*, 2015, **17**, 6577–6587.
12 Y. Nishiyama, M. Malon, Z. Gan, Y. Endo and T. Nemoto, *J. Magn. Reson.*, 2013, **230**, 160–164.
13 I. Haies, J. Jarvis, L. J. Brown, I. Kuprov, P. T. F. Williamson and M. Carravetta, *Phys. Chem. Chem. Phys.*, 2015, **17**, 23748–23753.
14 Z. H. Gan, *J. Am. Chem. Soc.*, 2006, **128**, 6040–6041.
15 Z. H. Gan, *J. Magn. Reson.*, 2007, **184**, 39–43.
16 Z. H. Gan, J. P. Amoureux and J. Trebosc, *Chem. Phys. Lett.*, 2007, **435**, 163–169.
17 S. Cavadini, A. Abraham and G. Bodenhausen, *J. Magn. Reson.*, 2008, **190**, 160–164.
18 S. Cavadini, A. Abraham, S. Ulzega and G. Bodenhausen, *J. Am. Chem. Soc.*, 2008, **130**, 10850–10851.

19 S. Cavadini, S. Antonijevic, A. Lupulescu and G. Bodenhausen, *ChemPhysChem*, 2007, **8**, 1363–1374.
20 S. Cavadini, S. Antonijevic, A. Lupulescu and G. Bodenhausen, *J. Magn. Reson.*, 2006, **182**, 168–172.
21 S. Cavadini, A. Lupulescu, S. Antonijevic and G. Bodenhausen, *J. Am. Chem. Soc.*, 2006, **128**, 7706–7707.
22 S. Cavadini, V. Vitzthum, S. Ulzega, A. Abraham and G. Bodenhausen, *J. Magn. Reson.*, 2010, **202**, 57–63.
23 V. Vitzthum, M. A. Caporini and G. Bodenhausen, *J. Magn. Reson.*, 2010, **205**, 177–179.
24 V. Vitzthum, M. A. Caporini, S. Ulzega and G. Bodenhausen, *J. Magn. Reson.*, 2011, **212**, 234–239.
25 V. Vitzthum, M. A. Caporini, S. Ulzega, J. Trebosc, O. Lafon, J. P. Amoureux and G. Bodenhausen, *J. Magn. Reson.*, 2012, **223**, 228–236.
26 Y. L. Hong, T. Asakura and Y. Nishiyama, *ChemPhysChem*, 2018, **19**, 1841–1845.
27 G. N. M. Reddy, M. Malon, A. Marsh, Y. Nishiyama and S. P. Brown, *Anal. Chem.*, 2016, **88**, 11412–11419.
28 D. Carnevale, X. Ji and G. Bodenhausen, *J. Chem. Phys.*, 2017, **147**, 184201.
29 A. S. Tatton, T. N. Pham, F. G. Vogt, D. Iuga, A. J. Edwards and S. P. Brown, *Mol. Pharmaceutics*, 2013, **10**, 999–1007.
30 A. S. Tatton, T. N. Pham, F. G. Vogt, D. Iuga, A. J. Edwards and S. P. Brown, *CrystEngComm*, 2012, **14**, 2654.
31 Y. Nishiyama, Y. Endo, T. Nemoto, H. Utsumi, K. Yamauchi, K. Hioka and T. Asakura, *J. Magn. Reson.*, 2011, **208**, 44–48.
32 J. A. Jarvis, I. M. Haies, P. T. F. Williamson and M. Carravetta, *Phys. Chem. Chem. Phys.*, 2013, **15**, 7613–7620.
33 D. Marion, M. Ikura, R. Tschudin and A. Bax, *J. Magn. Reson.*, 1989, **85**, 393–399.
34 A. E. Bennett, J. H. Ok, R. G. Griffin and S. Vega, *J. Chem. Phys.*, 1992, **96**, 8624–8627.
35 F. Delaglio, S. Grzesiek, G. W. Vuister, G. Zhu, J. Pfeifer and A. Bax, *J. Biomol. NMR*, 1995, **6**, 277–293.
36 W. F. Vranken, W. Boucher, T. J. Stevens, R. H. Fogh, A. Pajon, P. Llinas, E. L. Ulrich, J. L. Markley, J. Ionides and E. D. Laue, *Proteins*, 2005, **59**, 687–696.
37 P. Bertani, J. Raya and B. Bechinger, *Solid State Nucl. Magn. Reson.*, 2014, **61–62**, 15–18.
38 H. J. Hogben, M. Krzystyniak, G. T. P. Charnock, P. J. Hore and I. Kuprov, *J. Magn. Reson.*, 2011, **208**, 179–194.
39 M. Profeta, F. Mauri and C. J. Pickard, *J. Am. Chem. Soc.*, 2003, **125**, 541–548.
40 S. J. Clark, M. D. Segall, C. J. Pickard, P. J. Hasnip, M. J. Probert, K. Refson and M. C. Payne, *Z. Kristallogr.*, 2005, **220**, 567–570.
41 C. J. Pickard and F. Mauri, *Phys. Rev. B: Condens. Matter Mater. Phys.*, 2001, **63**, 245101.
42 J. R. Yates, C. J. Pickard and F. Mauri, *Phys. Rev. B: Condens. Matter Mater. Phys.*, 2007, **76**, 024401.
43 S. Li, L. Zhou, Y. Su, B. Han and F. Deng, *Solid State Nucl. Magn. Reson.*, 2013, **54**, 13–17.
44 S. Li and M. Hong, *J. Am. Chem. Soc.*, 2011, **133**, 1534–1544.
45 D. K. Lee, Y. F. Wei and A. Ramamoorthy, *J. Phys. Chem. B*, 2001, **105**, 4752–4762.
46 Y. F. Wei, D. K. Lee, A. E. McDermott and A. Ramamoorthy, *J. Magn. Reson.*, 2002, **158**, 23–35.
47 J.-S. Lee and A. K. Khitrin, *Concepts Magn. Reson., Part A*, 2008, **32**, 56–67.
48 R. E. Stark, R. A. Haberkorn and R. G. Griffin, *J. Chem. Phys.*, 1978, **68**, 1996.
49 M. D. Esrafili, H. Behzadi and N. L. Hadipour, *Biophys. Chem.*, 2008, **133**, 11–18.
50 M. Bak, R. Schultz, T. Vosegaard and N. C. Nielsen, *J. Magn. Reson.*, 2002, **154**, 28–45.
51 M. K. Pandey and Y. Nishiyama, *J. Magn. Reson.*, 2015, **258**, 96–101.
52 C. A. Mcdowell, A. Naito, D. L. Sastry and K. Takegoshi, *J. Magn. Reson.*, 1986, **69**, 283–292.
53 S. E. Ashbrook, S. Antonijevic, A. J. Berry and S. Wimperis, *Chem. Phys. Lett.*, 2002, **364**, 634–642.
54 M. J. Thrippleton, M. Cutajar and S. Wimperis, *Chem. Phys. Lett.*, 2008, **452**, 233–238.
55 M. Chan-Huot, S. Wimperis, C. Gervais, G. Bodenhausen and L. Duma, *ChemPhysChem*, 2015, **16**, 204–215.
56 J. A. Jarvis, I. Haies, M. Lelli, A. J. Rossini, I. Kuprov, M. Carravetta and P. T. F. Williamson, *Chem. Commun.*, 2017, **53**, 12116–12119.